ADVANCED HEALTHCARE MATERIALS
www.advhealthmat.de

TGase-Enhanced Microtissue Assembly in 3D-Printed-Template-Scaffold (3D-MAPS) for Large Tissue Defect Reparation

Hongsheng Yu, Zhifeng You, Xiaojun Yan, Wei Liu, Zhirui Nan, Dan Xing, Chenyu Huang, and Yanan Du**

Engineering large and functional tissue constructs with complex structures (e.g., external ear or nose) for reparation and reconstruction of tissue defects remains one of the major challenges in regenerative medicine, which demands abundant cell sources, advanced biofabrication schemes, and satisfactory integration with the host for long-term efficacy post implantation. Here the 'Microtissue Assembly in 3D-Printed-template-Scaffold' (3D-MAPS), as a platform technology to rapidly fabricate centimeter-sized functional tissue constructs with complex structures, is developed. 3D-MAPS facilitates bottom-up assembly of large-scale manufactured microtissues within the 3D-printed hollow polymeric templates with pre-defined architectures. The assembly and fusion of 2×10^6 mesenchymal stem cell–based microtissues within the defined 3D-printed template is further enhanced by addition of a natural protein crosslinker (i.e., transglutaminase (TGase)), and thereby achieves construction of centimeter-sized tissue with high cell viability and mechanical stability in vitro within 30 min. Further in vivo implantation of the 3D-MAPS-fabricated ear-like tissue construct in rabbit models assisted by flap prefabrication technique results in increased structural vascular support and strengthened functional survival. Thus, the TGase-enhanced 3D-MAPS demonstrates its potential and feasibility as a powerful biofabrication platform for tissue engineering application.

Progress in bottom-up tissue engineering[1] and 3D bioprinting[2–4] offers versatile tools to build tissue constructs by assembly or printing of cell/biomaterial-containing module or ink. However, for the reparation or reconstruction of large tissue defects using defined architectures (e.g., ear or nose defects), the challenges remain multifaceted, such as how to obtain the sufficient amount of cells with high quality, how to achieve rapid and precise fabrication of large tissue constructs without interfering the huge amount of live cells; and how to maintain the pre-defined tissue architectures overtime while creating an amiable cellular microenvironment.[5,6] Additionally, lack of vascular support from endogenous blood vessels aggravates the difficulties in survival and functionalities of the tissue construct after in vivo implantation.[7]

Here, we integrate bottom-up tissue engineering with 3D-printing for rapid fabrication of large and functional tissue constructs by assembling large-scale manufactured microtissues within the 3D-printed hollow polymeric templates with pre-defined architectures (e.g., nose or ear-like structure). The purpose of 'Microtissue Assembly in 3D-Printed-template Scaffold' (3D-MAPS) platform (Figure 1) is to combine the advantages in the precise prototyping capacity of 3D printing with the large-scale manufacture capacity of microtissues as amiable cellular niches, in which all the components actively participate in the ear or nose-like cartilage tissue engineering. Transglutaminase (TGase) is also introduced as an enzymatic crosslinker to glue microtissues for rapid fusion into tissue assembly within the 3D-printed template. Additionally, based on the flap prefabrication approach from a plastic

Dr. H. Yu, Dr. Z. You, Dr. Z. Nan, Prof. Y. Du
Department of Biomedical Engineering, School of Medicine
Tsinghua-Peking Center for Life Sciences, MOE Key Laboratory of Bioorganic Phosphorus Chemistry and Chemical Biology
Tsinghua University
Beijing 100084, China
E-mail: duyanan@tsinghua.edu.cn

The ORCID identification number(s) for the author(s) of this article can be found under https://doi.org/10.1002/adhm.202000531

DOI: 10.1002/adhm.202000531

Dr. C. Huang
Department of Dermatology
Beijing Tsinghua Changgung Hospital
School of Clinical Medicine
Tsinghua University
Beijing 102218, China
E-mail: huangchenyu@tsinghua.edu.cn

Dr. X. Yan, Dr. W. Liu
Beijing CytoNiche Biotechnology Co. Ltd.
Beijing 100195, China

Dr. D. Xing
Arthritis Clinic and Research Center, Peking University People's Hospital
Peking University
Beijing 100044, China

© 2020 Wiley-VCH GmbH

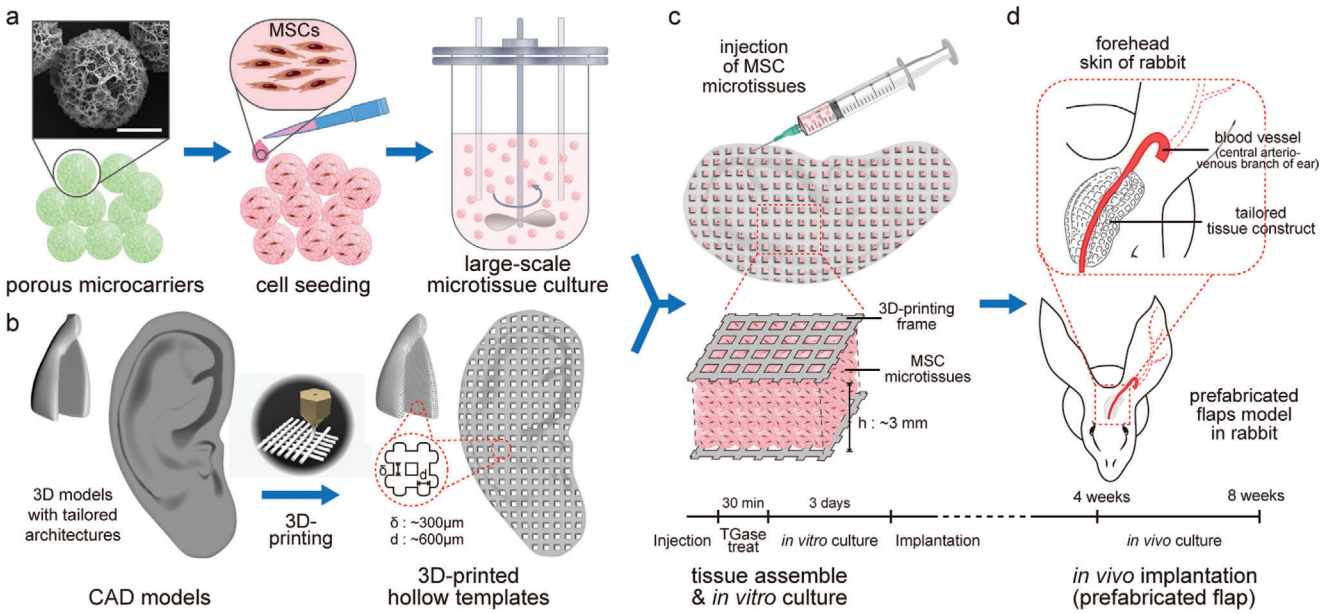

Figure 1. Schematic illustration to describe the technological process of 3D-MAPS platform. a) Large-scale expansion of MSC microtissues. b) 3D printing model design and fabrication. c) TGase assisted tissue assembly and in vitro culture. d) In vivo implantation. Scale bar, 100 μm.

surgery's perspective,[8,9] the endogenous vascular sprouting and ingrowth into the recipient 3D-MAPS were potentiated along the pre-designed microchannel within the construct, which guarantees the vascular perfusion through the entire cartilage construct meanwhile facilitating subsequent surgical transfer of the vascularized tissues for defect repair and/or reconstruction.

The clinical applications of human mesenchymal stem cells (MSCs) for regenerative therapy of various degenerative diseases including cartilage and bone defects have been widely acknowledged.[10,11] In this study, adipose MSC-based microtissues were formed as previously described,[12] where MSCs derived from adipose tissue were 3D cultured in the gelatin-based porous microcarriers (Figure 2a,f). Taking advantage of the large-scale in vitro bioreactor culture system (Figure 2b), we could achieve large scale microtissue manufacture (up to 2×10^6 microtissues). Inside that system, MSCs expanded in quantities from 5×10^6 to 9.1×10^7 (Figure 2c), without significant loss in the quality of their stem cell properties within a relatively short time (4 days, Figure 2d), the achievement of which had long been a challenge and obstacle in MSC-based therapies.[13] During expansions, the porous microcarriers constituted the beneficial microenvironment to facilitate MSC adhesion and proliferation meanwhile maintaining the cell viability above 95% (Figure 2c–g). After 4-day in vitro culture, significant ECM deposition was found on the porous surface (Figure 2f). Flow cytometry results demonstrated that MSCs in the microtissues retained their immunophenotype during the in vitro 3D culture with high expressions of CD73, CD90, CD105 and low expressions of CD11b, CD14, CD19, CD34, and HLA-DR (Figure 2h and Figure S1, Supporting Information).[14]

To satisfy the demand in rapid fabrication of tissues with tailored geometry while maintaining efficient mass transfer, the template was modified to be hollow and meshed (pore size ≈300 μm) in structures (Figure 1). The MSC microtissues were then injected into the 3D-printed-template-scaffold for large-scale tissue assembly. Further, considering the fact that TGase is a Ca^{2+}-dependent enzyme which catalyzes the cross-link between side chains of lysine and glutamine and has been widely used as a crosslinking agent for biomaterials fabrication and as a surgical adhesive at clinic,[15,16] TGase was applied accordingly as a glue to facilitate the microtissue assembly within the 3D-printed-template-scaffold (3D-MAPS) and thereby promote the tissue assembly during in vitro culture. To verify the feasibility of the 3D-MAPS platform for large-scale tissue assembly, we examined next the TGase-assisted microtissue assembly in the 3D-printed hollow templates with simplified shapes (Figure 3a). Compared with free culture microtissues and assembled tissue without TGase treatment, our TGase-treated tissue showed a more integrated structure while maintaining high cell viability (Figure 3c,d). Appropriate TGase treatment (≈30 min, 2 mg mL^{-1}) further promoted the cell growth and the deposition of ECM between adjacent microtissues (Figure 3d,e) which in return increased the mechanical stability of the assembled tissue while reserving the macro-scale porous structure to allow metabolism of the inner tissue (Figure 3e and Figure S2, Supporting Information). In contrast, the MSCs cultured in the bulk material with the same dimensions and compositions demonstrated significant cell necrosis in the central zone (Figure 3c) instead. Based on these findings, the tissue with more complex geometrical requirements, such as nose or ear-like structures (Figure 3b), was then tried within the 3D-MAPS platform. As demonstrated in the micro-CT results, the microtissues could have a high filling rate even in nose or ear-like structures with complex geometries (Figure 4a–d). The presentation of MSCs in microtissues significantly attenuates the foreign body reaction in the subcutaneous implantation model, while the groups without microtissues or without MSCs shows obvious fibrous capsule development (Figure 4e).

© 2020 Wiley-VCH GmbH

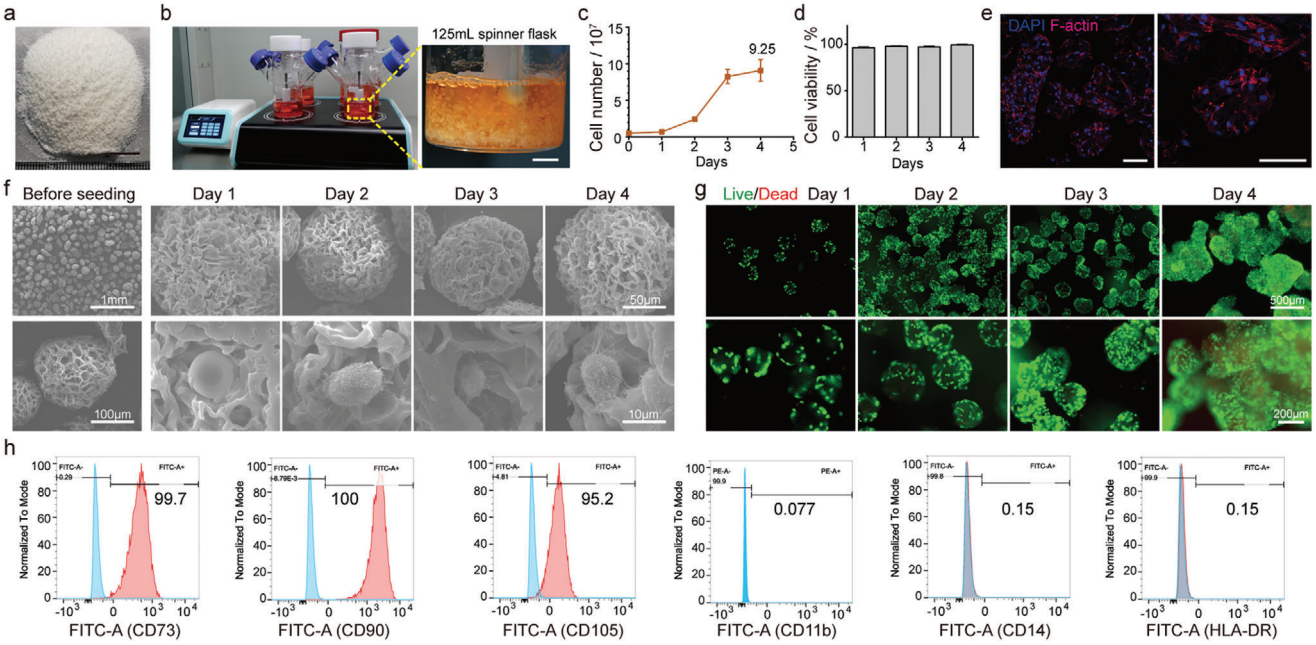

Figure 2. Large scale culture of MSCs in micro-tissue. a) Images of gelatin-based porous microcarriers. Scale bar, 1 cm. b) Spinner flask based 3D cell culture system for MSCs in microtissue. Scale bar, 1 cm. c,d) Cell proliferation and viability testing in microtissues during 4 days culturing. e) Confocal images of MSCs in the porous microcarriers. Scale bar, 100 μm. f) SEM images of microtissue. g) Live/Dead staining of MSCs in microtissues, scale bar 100 μm. h) FACS detection of markers of MSCs in microtissues after 4 days culturing.

The assembled tissue with auricular structure was chosen for in vivo implantation to verify the feasibility of the 3D-MAPS platform in repairing large tissue defects. To promote tissue survival after implantation, we developed a surgical strategy to allow endogenous vascular sprouting and ingrowth into the recipient 3D-MAPS. The auricular central arteriovenous branch was ligated distally, reversed at the ear root, and implanted into the forehead through the subcutaneous tunnel. On the forehead, the implanted branch was then placed into the tunnel within the 3D template (Figure 4f,h). The width, length, and depth of the tunnel was tailored for the implanted blood vessels to guarantee their full contact and close adherence with the template, allowing endothelial ingrowth and the following angiogenesis, meanwhile successfully avoiding potential damages. The auricular central arteriovenous branch was transferred into the tailored 3D template tunnel accordingly through these flap prefabrication techniques. The retained long ligation sutures at the end of the branch were used to fix the vessels on the one hand to the 3D scaffold and on the other hand to the dermal skin. Location and tension of such fixations were controlled suitable to avoid potential damages to the vessels (Figure 4f,h and Figure S3, Supporting Information). It was through these surgical procedures, can the implanted vessels functioned to guarantee vascular supply to the microtissues through their spouting from the branch, meanwhile serving as the fishing rod to harvest and elevate the whole system for potential transfer application into other recipient sites. Two weeks later, the assembled tissue demonstrated ear contour in the implanted recipient site with normal hair-growth, indicating the persistence of blood supply in the flap. The microtissues in the template also showed denser structures (Figure 4i) with significantly increase in the tissue stiffness (Figure 4j) and bold vessels ingrowth (Figure 4g). Although the 3D-MAPS tissues used for in vivo implantation consist of undifferentiated MSCs, the safranin O and fast green staining implied differentiation tendency of MSCs to chondrogenic lineage in the flap prefabrication model two weeks after implantation (Figures S4 and S5, Supporting Information), highlighting the differentiation potential of the 3D-MAPS tissue to form organ-specific tissue in vivo. Alternatively, the ear or nose-like 3D-MAPS tissue could be pre-induced in the chondrogenic differentiation medium to form cartilage-like tissue before in vivo implantation (Figure S6, Supporting Information), which is expected to further improve the efficacy for repairing the auricle or nose defects. In the future, the 3D-MAPs platform can be potentially applied to engineer large and functional tissue constructs with complex structures for reparation and reconstruction of various tissue defect. 3D-printing materials with tailored biochemical and biophysical properties could be chosen in demand according to the natural properties of specific tissues to be repaired and restored.

In summary, we developed a 3D-MAPS platform for rapid and efficient repairing of large tissue defects by assembling large-scale manufactured microtissues within the 3D-printed hollow templates with pre-defined architectures. The 3D-MAPS platform effectuated rapid and precise fabrication of large tissue constructs without undesired effects on the cell viability for the microtissues. TGase, which was introduced as an enzymatic crosslinker, significantly accelerated the fusion of microtissues into tissue assembly within the 3D-printed template. Additionally, the flap prefabrication approach provided full blood supply to the microtissues within the large template through the vascular spouting from the implanted arteriovenous branch, which also served as the fishing rod to harvest and elevate the whole

© 2020 Wiley-VCH GmbH

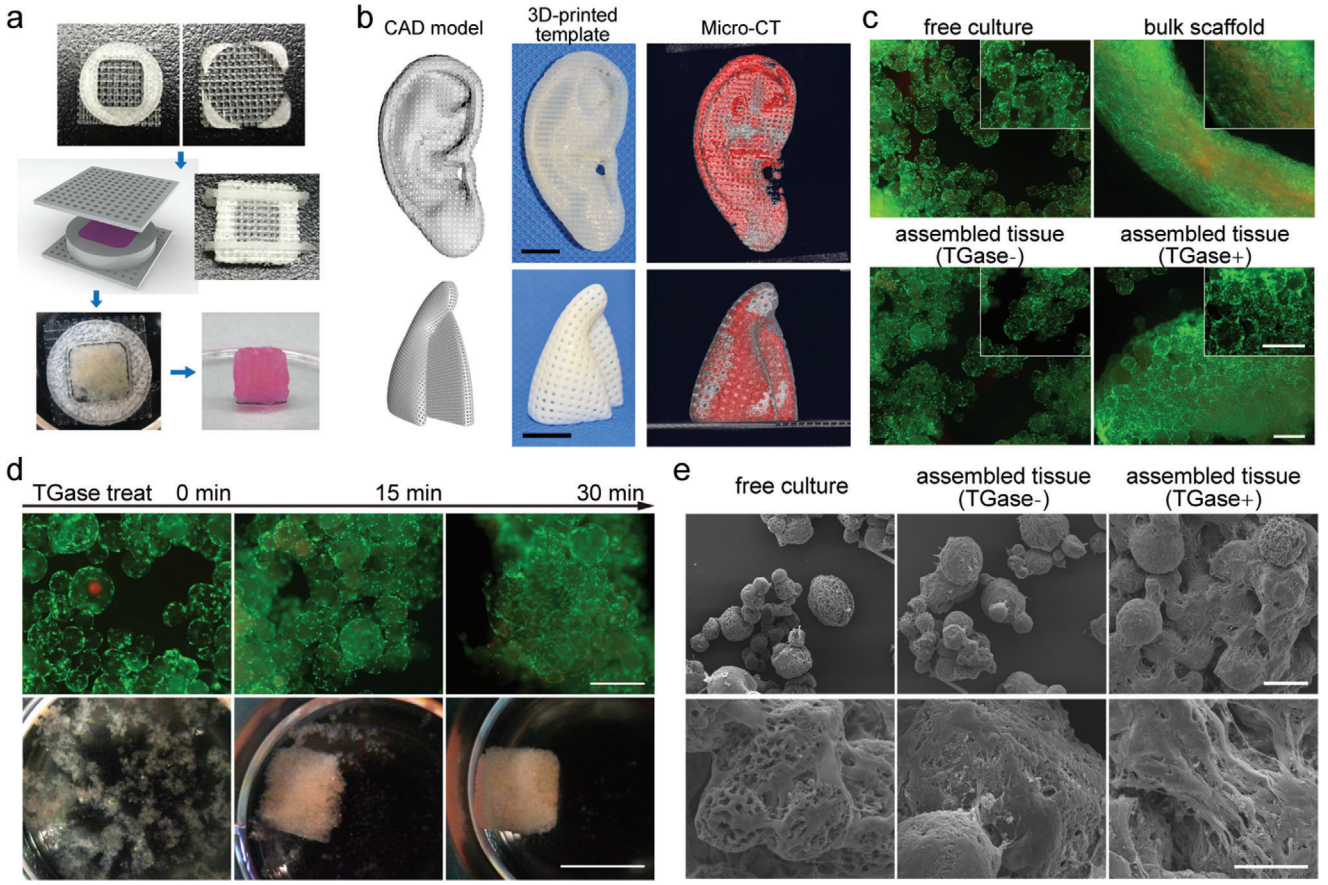

Figure 3. TGase-assisted tissue assembly and in vitro culture. a) Technological process of TGase-assisted tissue assembly in the simplified 3D-Printed-template-scaffold. b) 3D-printed hollow templates with ear and nose-like structure. (from left to right: the CAD design in 3DMAXs, the appearance of 3D printed templates and the reconstruction results after filling the template with microtissues. Red signal in MicroCT, microtissues. White signal in MicroCT, 3D printed templates. Scale bar, 1 cm). c) Cell viability of MSCs after 3 days in vitro culture within the 3D printed templates shown by the live-dead staining. Scale bar, 500 μm. d) Stability of microtissue assembly under different conditions of TGase treatment after taking out from the 3D printed templates. Top, live-dead staining. Bottom, the appearance of the whole tissue. Scale bar, 500 μm (up), 5 mm (down). e) SEM images of the assembled tissue after 3 days in vitro culture within the 3D printed templates. Scale bar, 200 μm (up), 50 μm (down).

system for potential transfer application into other recipient sites.

Experimental Section

3D-Printing and Model Design: 3D printer (AOD3D, China) and Flexifil filament (a rubber-like thermoplastic co-polyester, Flexifil is a registered trademark of the company FormFutura, Netherlands) were used in this study for the fabrication of 3D-printed polymeric template.' were used in this study for the fabrication of 3D-printed polymeric template. The side length of the square holes on the hollow template was optimized to ≈300 μm to allow the material exchange meanwhile avoiding any leakage of microtissues. The 3D-printed templates were designed with 3D Studio Max and Solidworks (Autodesk).

Cell Inoculation and Expansion on 3D TableTrix in Spinner Flask: MSCs were cultured on 3D TableTrix (F01, CytoNiche Biotech, China), a tablet which disperse into a hundred thousand gelatin-based microcarriers upon introduction to aqueous solution.[17] 5 tablets of 3D TableTrix (giving a total of 5×10^5 microcarriers) with 40 mL culture medium (M001, Viral Therapy Technologies, China) and 5×10^6 adipose-derived MSCs (human) were introduced into a sterile 125 mL spinner flask (SF125, CytoNiche Biotech, China). The spinner flask was then placed on a 3D FloTrix miniSPIN system (M1, CytoNiche Biotech, China) that was set up inside a cell culture incubator (CCL1708-8, ESCO, Singapore). The miniSPIN system was programmed to perform 58 cycles of 60 rpm × 5 min and 0 rpm × 20 min agitation (about a total of 24 h), then followed by constant speed of 60 rpm agitation for an additional 72 h, for a total culture time of 96 h. 20 mL fresh culture medium was supplemented to the spinner flask via the sidearm at $t = 72$ h after inoculation. Samples were taken each day to monitor cell growth. Cells on microcarriers were enumerated by dissolving microcarriers with 3D FloTrix Digest (CNR001-500, CytoNiche Biotech, China) reagent at a ratio of 0.15 mL mg^{-1} microcarriers for 30 min at 37 °C. Cell numbers were counted with an automatic cell counter (Countstar Biotech, ALIT Life Science, China) and viability were evaluated with Trypan Blue exclusion assay.

Flow Cytometry: Immunophenotypes of MSCs were analyzed by flow cytometry of cells stained with pre-conjugated antibodies. MSCs were harvested from microcarriers by dissolving microcarriers using 3D FloTrix Digest. They were then stained with CD73-FITC (344 015), CD90-FITC (3281-7), CD105-FITC (800 505), CD45-PE (304 007), CD34-FITC (343 503, Biolegend, US), CD14-FITC(301 803), CD19-PE (302 207), HLA-DR-FITC (307 603, all antibodies above from Biolegend, US), and CD11b-PE (561 001, BD Biosciences, US). More than 5×10^4 total events were

 © 2020 Wiley-VCH GmbH

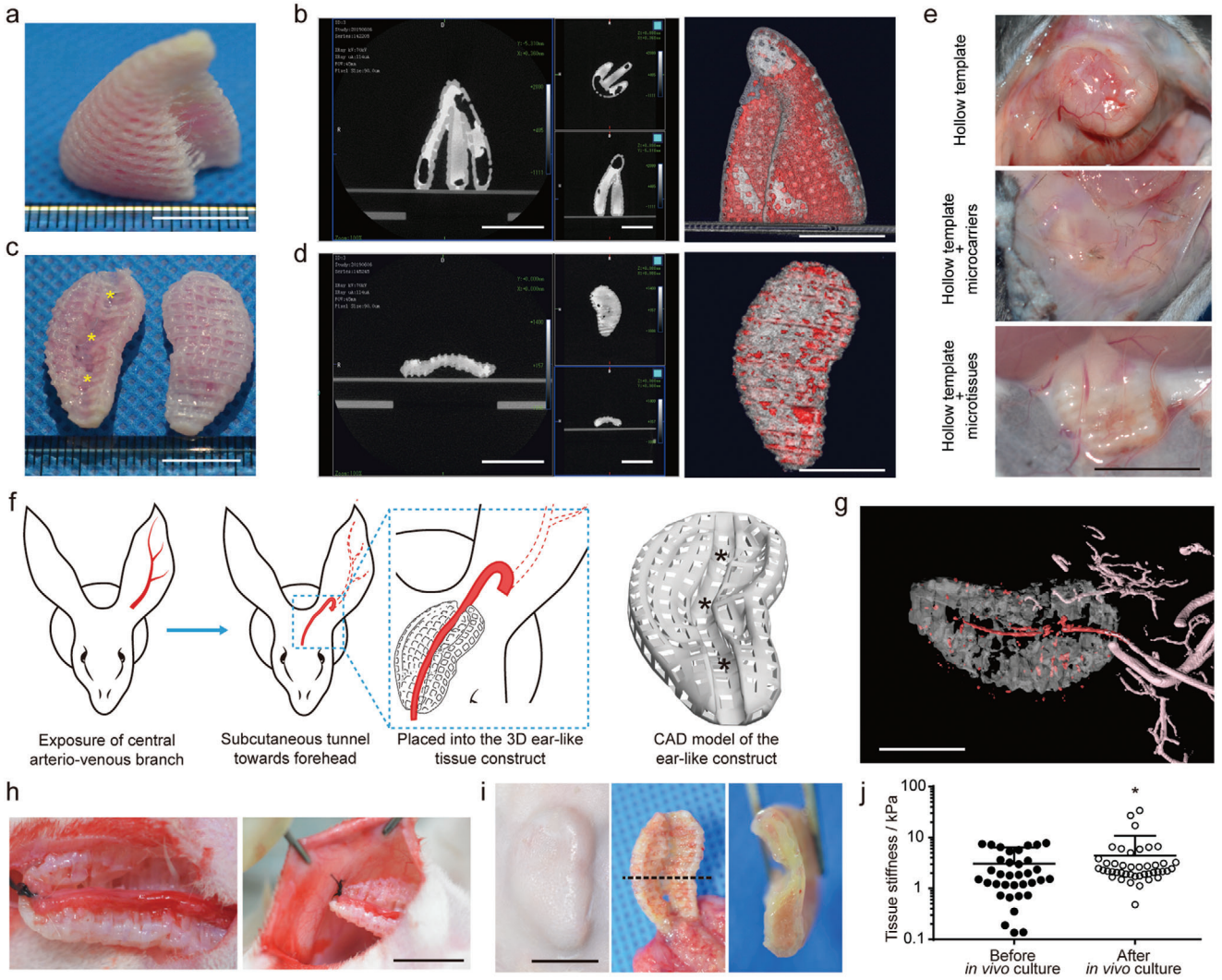

Figure 4. In vivo implantation of 3D-MAPS tissue in flap prefabrication animal model and the evaluation. a) 3D-MAPS tissue with auricular structure. b) CT image of 3D-MAPS tissue with nose-like structure. Left, section view from different coordinate planes. Right, 3D image (red signal indicates the microtissues). c) 3D-MAPS tissue with ear structure, * indicates tailored tunnel on the ear structure. d) CT image of 3D-MAPS tissue with the auricular structure before in vivo implantation. Scale bar (a–d), 1 cm. e) Images of 3D-MAPS tissue 2 weeks after the implantation in mouse models. Scale bar, 1 cm. f) Schematic illustration of the flap prefabrication rabbit model process, * indicates the tailored tunnel on the ear structure. g) CT image of 3D-MAPS tissue and the blood perfusion after two weeks implantation. Red signal indicates the blood vessels with blood perfusion inside the 3D-MAPS tissue. Light red signal indicates peripheral blood perfusion. And grey signal indicates the 3D-MAPS tissue. h) The implanted auricular central arteriovenous branch was placed into the tailored long and loose tunnel within the 3D template filled with microtissues, and carefully fixed at their end onto the template. i) Images of 3D-MAPS tissue after 2 weeks implantation in rabbit model. j) Tissue stiffness of 3D-MAPS tissue before and after 2 weeks implantation in rabbit model (*, $p = 0.0493$).

acquired on an Aria SORP FACS (BD Biosciences, US) and analyzed using FlowJo Ver. 10.1 (BD Biosciences, US).

TGase Assisted Micro Tissue Assembly: MSCs microtissues cultured in the large-scale in vitro culture system for 5 days was used for tissue assembly. 3D-printed templates were autoclaved and immersed in PBS for at least 1 day before use. Microtissues suspension was slowly injected into the 3D-printed template (syringe size of 16 gauge). Then the filled template was flushed using PBS and immersed into 2 wt% TGase solution in DMEM. After 30 min long incubation at 37 °C, the template was flushed with PBS again to remove the residual TGase and then cultured in MSC growth medium for another 3 days.

Flap Prefabrication Animal Model: All animal protocols used in this study were approved by the Institutional Animal Care and Use Committee (IACUC) of Tsinghua University and performed following guidelines of the IACUC (Animal Protocol Number: 19-DYN1). The laboratory animal facility has been accredited by Association for Assessment and Accreditation of Laboratory Animal Care International (AAALAC). Humane treatment of all research animals was assured. Eight male New Zealand white rabbits (each with 2.5 kg in bodyweight) were used in the animal experiments. The dorsal side of the ear was totally depilated under general anesthesia with ketamine (0.2 mg kg^{-1}). The 10 cm long incision was made along the auricular central arteriovenous branch. Those vessels were then ligated and cut at the distal end. After full dissection, the vessels were separated and reversed at the ear root, then implanted into the forehead through the subcutaneous tunnel. On the forehead, the implanted auricular central arteriovenous branch was placed into the tailored long and

© 2020 Wiley-VCH GmbH

loose tunnel within the 3D template filled with microtissues, and carefully fixed on the template to guarantee their full contact and close adherence, and thereby allow endothelial ingrowth and the following angiogenesis. Two months later, the rabbit was sacrificed. And the implant along with the embedded vessels and peripheral tissue were harvested for histological examinations.

Subcutaneous Transplantation in Mouse: The 8-week-old male C57BL/6 mice were anesthetized with 2.5% avertin, and then the hollow template, hollow template loaded with empty microcarriers, or hollow template loaded with assembled microtissues were subcutaneously implanted into the mice for 2 weeks before characterization ($N = 3$ for each group).

Micro-CT: The 3D-printed template was fixed in 4% paraformaldehyde solution after 3-days in vitro culture. The samples were immersed in 15% meglumine diatrizoate solution for 10 min just before imaging. For the imaging of in vivo sample, after sacrifice, 40 mL heparin sodium saline and 20 mL developing agent (10 wt% $BaTiO_3$ microparticles suspension in 60% natural Latex) were slowly injected into the common carotid artery of the rabbit. The in vivo samples were fixed in 4% paraformaldehyde solution and stored at 4°C before imaging. Quantum GX microCT (PerkinElmer, US) was used for micro-CT imaging with 114 µA X-ray current and 70 kV X-ray voltage. The results were visualized in ImageJ (NIH, US).

Atomic Force Microscopy: The measurement of tissue stiffness for 3D-MAPS tissue before and after implantation was achieved by an AFM module Nanowizard (JPK Instruments). Silicon tipless cantilever (ARROW-TL1-50, NANOWORLD) with a nominal spring constant of 0.03 N m^{-1} and a silicon microbead (4 µm in diameter) attached on the cutting edge was used for operating force measurement. Hertz-fit model was used for data processing on JDP software (JPK Instruments).

Supporting Information

Supporting Information is available from the Wiley Online Library or from the author.

Acknowledgements

H.Y. and Z.Y. contributed equally to this work. This work was financially supported by the National Key R&D Program of China (Grant No. 2016YFC1000810).

Conflict of Interest

Y.D. is the scientific advisor. X.Y. and W.L. are employees of Beijing CytoNiche Biotechnology Co. Ltd. The other authors declare that we have no financial and personal relationships with other people or organizations that can inappropriately influence our work, there is no professional or other personal interest of any nature or kind in any product, service and/or company that could be construed as influencing the position presented in the manuscript entitled.

Keywords

3D printing, bottom-up tissue engineering, microtissues

Received: April 1, 2020
Revised: June 30, 2020
Published online:

[1] D. L. Elbert, *Curr. Opin. Biotechnol.* **2011**, *22*, 674.
[2] C. Xu, G. Dai, Y. Hong, *Acta Biomater.* **2019**, *95*, 50.
[3] C. Mandrycky, Z. Wang, K. Kim, D. Kim, *Biotechnol. Adv.* **2016**, *34*, 422.
[4] P. Bajaj, R. M. Schweller, A. Khademhosseini, J. L. West, R. Bashir, *Annu. Rev. Biomed. Eng.* **2014**, *16*, 247.
[5] D. A. Bichara, N. A. O'Sullivan, I. Pomerantseva, X. Zhao, C. A. Sundback, J. P. Vacanti, M. A. Randolph, *Tissue Eng. Part B Rev.* **2012**, *18*, 51.
[6] L. Nayyer, K. H. Patel, A. Esmaeili, R. A. Rippel, M. Birchall, G. O'Toole, P. E. Butler, A. M. Seifalian, *Plast. Reconstr. Surg.* **2012**, *129*, 1123.
[7] A. von Bomhard, J. Veit, C. Bermueller, N. Rotter, R. Staudenmaier, K. Storck, H. N. The, *PLoS One* **2013**, *8*, 71667.
[8] S. T. Yao, *Plast. Reconstr. Surg.* **1982**, *69*, 568.
[9] J. J. Pribaz, N. A. Fine, *Clin. Plast. Surg.* **2001**, *28*, 261.
[10] S. Wakitani, T. Mitsuoka, N. Nakamura, Y. Toritsuka, Y. Nakamura, S. Horibe, *Cell Transplant.* **2004**, *13*, 595.
[11] H. A. Awad, M. Q. Wickham, H. A. Leddy, J. M. Gimble, F. Guilak, *Biomaterials* **2004**, *25*, 3211.
[12] Y. Li, W. Liu, F. Liu, Y. Zeng, S. Zuo, S. Feng, C. Qi, B. Wang, X. Yan, A. Khademhosseini, J. Bai, Y. Du, *Proc. Natl. Acad. Sci. USA* **2014**, *111*, 13511.
[13] C. P. Ng, A. R. Sharif, D. E. Heath, J. W. Chow, C. B. Zhang, M. B. Chan-Park, P. T. Hammond, J. K. Chan, L. G. Griffith, *Biomaterials* **2014**, *35*, 4046.
[14] M. Dominici, K. Le Blanc, I. Mueller, I. Slaper-Cortenbach, F. Marini, D. Krause, R. Deans, A. Keating, D. Prockop, E. Horwitz, *Cytotherapy* **2006**, *8*, 315.
[15] F. Bertoni, N. Barbani, P. Giusti, G. Ciardelli, *Biotechnol. Lett.* **2006**, *28*, 697.
[16] D. I. Zeugolis, P. P. Panengad, E. S. Yew, C. Sheppard, T. T. Phan, M. Raghunath, *J. Biomed. Mater. Res. A* **2010**, *92*, 1310.
[17] X. Yan, K. Zhang, Y. Yang, D. Deng, C. Lyu, H. Xu, W. Liu, Y. Du, *Tissue Eng., Part C* **2020**, *26*, 263.

© 2020 Wiley-VCH GmbH